Visual Abstract

An experimental study and a proposed theoretical solution for the prediction of the ductile/brittle failure modes of reinforced concrete beams strengthened with external steel plates

Van-Hau Nguyen, Thanh Bui-Tien, Phe Van Pham, Long Nguyen-Ngoc*
Faculty of Civil Engineering, University of Transport and Communications, Cau Giay, Hanoi, Vietnam
nvhau@utc.edu.vn, btthanh@utc.edu.vn, phe.phamvan@utc.edu.vn; nguyenngoclong@utc.edu.vn

ABSTRACT. An experimental study is conducted and a theoretical solution is proposed in the present study to investigate the ductile/brittle failure mode of reinforced concrete (RC) beams strengthened with an external steel plate. In the present experimental study, 6 steel plate-strengthened RC beams and 1 non-strengthened RC beam are fabricated and tested under 4-point bending loads. Then, a new theoretical model is successfully developed to predict the rupture mechanism of the RC beams strengthened with external steel plates. The model is based on the observed experimental results regarding to crack formations, and it is can be used to determine the distance between vertical cracks and to quantitatively predict the ductile/brittle failure mode of plate-strengthened RC beams. The experimental study shows that the failure mode is commonly based on the sliding of concrete along with the external plate at a random location. This slip is limited between two vertical cracks, from which the maximum stresses in the external steel is determined. Through result validations, the stresses/strains in the soffit plate, crack distances, and system failure modes as predicted by the present theoretical solution are found to excellently agree with those of the previous and present experimental results. This study may help to improve the design of such plate-strengthened RC beams to target on a better ductile performance, that has not been addressed before.

KEYWORDS. External steel plate; Strengthening reinforcement concrete beam; Flexural reinforcement limit; Tension chord model; Ductile failure conditions.

OPEN ACCESS

Citation: Nguyen, V.-H., Bui-Tien, T., Pham, P. V., Nguyen-Ngoc, L., An experimental study and a proposed theoretical solution for the prediction of the ductile/brittle failure modes of reinforced concrete beams strengthened with external steel plates, Frattura ed Integrità Strutturale, 61 (2022) 198-213.

Received: 23.02.2022
Accepted: 27.04.2022
Online first: 10.05.2022
Published: 01.07.2022

INTRODUCTION

Strengthening of existing RC beams in buildings or bridges by using external bonding steel plates is gradually getting more attention to upgrade their load capacities [1]. Because steel plates often have a large elastic modulus and various thicknesses, they can typically meet structural strengthening requirements such as upgrading the system flexural and

shear strengths [1,2,3]. In addition, painting and galvanizing technologies make the steel durable against rust and meet all requirements of durability. As observed, recent results of flexural tests for reinforced concrete beams strengthened by external steel plates showed that their brittle failure mode was a relatively common phenomenon [1-3]. Although RC beams strengthened with an external steel plate can significantly increase the system flexural strength [5]; however, the system ductility, as observed through the beam deflection, was remarkably reduced [1-4][16][22][24]. In some studies, test results showed that the flexural strength could be doubled, but the midspan deflection was reduced to one-fifth [2][3] as samples Sb6, Sb4.5 in Fig. 1 of the study by Aykac et al. [3]. Furthermore, the debonding of the external steel plate from the concrete beam happens regularly at the rupture point as mentioned in several documents [6-13]. The delamination position takes place randomly either at the plate end or at the location where cracks happen [9]. This delamination leads to the fact that the RC beams were broken suddenly because the external plates do not contribute their capacity to the RC beam resistance. Based on such an unobvious scenario, several techniques were then proposed/developed to detect and prevent the debonding of the external steel plate, such as the studies of Liu et al [14] and Wojtczak et al. [15], Wu and Lu [7] and Sallam et al [8]. However, the above studies (i.e., [6-8]) might not fully address the rupture mechanism of such plate strengthened RC beams. As the ductility of a structure is an indispensable requirement, a deeper study regarding the rupture mechanism may become essential to avoid possible brittle ruptures of a plate strengthened RC structure.

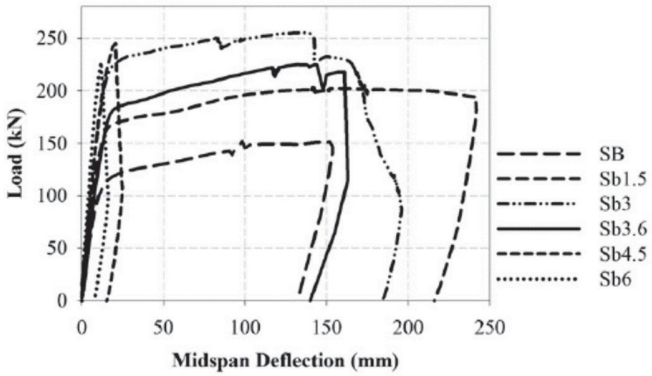

Figure 1: Load versus displacement of RC beam with external steel plate [3].

Quantification of the brittle failure in plate-strengthened RC beams has not been studied extensively and specifically. For reinforced concrete beams strengthened by external plates such as fiber-reinforced composite laminates (FRP) or steel plates, there may be an only guideline for brittle failure resistance conditions presented in ACI 440.2R, those were based on the studies of pulling tests of an external plate adhered with a concrete part [4][5][17][18] (as depicted in Fig. 2). Because a crack formation of RC beams under bending always exists, such a guideline based on the given experimental model may not able to apply to the plate-flexurally strengthened RC beams. Recent studies on the failure characteristics of RC beams bonded with external plates demonstrated the separation of the plate from the beam at plate ends or at the mid-span of the concrete beam. At the rupture, plate stresses reach a limit [2][20]. Since the existing RC beams usually appear crack, the maximum stresses in the steel may be determined. As a result, the stresses in the external plate in the ruptured state may be known. However, brittle failure conditions were not being thoroughly addressed and hence ductility is not guaranteed in the studies discussed above.

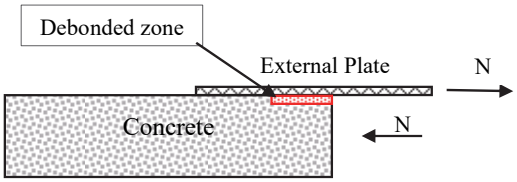

Figure 2: Experimental model to determine strength development length [4-7].

Based on the context, the present study is going to conduct an experimental study on the rupture mechanism of the plate-strengthened RC beams and propose a theoretical model to predict a crack formation, the distance between cracks, and the failure characteristics of such systems. The experiment study will be conducted based on relatively practical dimensions of

several RC beams strengthened with steel plates subjected to flexural loadings. Meanwhile, the theoretical model is going to investigate the mechanism of crack formation, the distance between cracks, and the failure characteristics of the plate-strengthened RC beams. The results of the proposed theory will be validated against those of the experimental study conducted in the present study and those presented in other experimental studies. Finally, an important (safe) limit of the RC beams strengthened with external steel plates will be proposed in the present study to ensure a plastic failure mode of the systems.

EXPERIMENTAL SETUP

Materials

Three specimens of structural plated steel, steel reinforcement, and 9 specimens of concrete were tested for the material properties. The mechanical tests are conducted according to ASTM A370-15 [16] and ASTM C39 [17] for the materials, respectively. The averaged test results are summarized in Tab. 1. In the fabrication of the steel-strengthened RC beams, steel plates are glued to the test beams by using Sika's epoxy adhesive Sikadur 752. This adhesive has compressive and tensile strengths of 50 MPa and 20MPa, respectively, which are higher than the strengths of concrete.

Fabrication of Test Specimens

Seven identical RC beams are fabricated based on the dimensions given in Fig.3. The beams have a span of $L_g = 2.0m$, a cross-section of $h \times b = 200mm \times 150mm$. The longitudinal steel reinforcements include two $\phi 16\,mm$ rebars in tension and two $\phi 8\,mm$ rebars in compression. Stirrups are created by using $\phi 8\,mm$ steels and they are arranged at equal distances of $50mm$ along the beams. The first RC beam is denoted as D0 (i.e., a reference beam) in which no strengthening is applied. The six remaining RC beams are denoted as from D1 to D6 in which they are strengthened with identical steel plates (Fig. 3). The steel plates have a length of $L_p = 1.9m$, a width of $b = 150mm$, and a thickness of $h_p = 2.8mm$.

The steel plates are bonded to the RC beams by using high viscous epoxy resin (i.e., Sikadur 752). Gluing is based on the injection molding method [18, 19]. The method ensures that the gaps between the steel plate and concrete beam are fully filled with the epoxy without voids so that the sliding resistance of the concrete is maximally mobilized. The method may include three basic steps. Step 1: Attach the steel plate to the bottom surface of the RC Beam, Step 2: Use a low viscous resin (e.g., Sikadur 731) to seal outer gaps between the plate boundary edges and the concrete to form a sealed chamber. Step 3: To install an inlet valve at one end of the steel plate (in the longitudinal direction), and install an outlet valve at another end of the steel plate, then the high-pressure pump is installed to inject the high viscous epoxy resin into the remaining gaps between the steel plate and the concrete beam (inside the chamber). The inlet valve only allows the resin to flow in one direction. The outlet valve is unlocked to ensure that the resin can be flowed out. After seeing a small amount of the resin flow out from the outlet valve, the outlet valve is locked while the inlet valve is opened for about five minutes so that resin can be fully pumped/filled in all voids in the chamber. After that, the pumping is stopped and the system remains for 24 hours so that the resin can be fully cured.

As discussed, because the target of this work is to observe the possible brittle failure modes of the beams under bending, all of the strengthened RC beams are thus fabricated based on the same material and reinforcement arrangements to justify the failure modes maybe not like those observed in studies [4][16-18].

No.	Parameters (notation)	Unit	Test value
1	Cube concrete strength (f_c)	(MPa)	33.0
2	Yield strength of steel bar (f_y)	(MPa)	446.2
3	Ultimate strength of steel bar (f_u)	(MPa)	603.6
4	Yield strength of steel plate (f_{py})	(MPa)	380.0
5	Ultimate strength of steel plate (f_{pu})	(MPa)	412.0
6	Elastic modulus of steel bar (E_s)	(MPa)	205,000.0
7	Elastic modulus of steel plate (E_p)	(MPa)	195,000.0

Table 1: Mechanical properties of testing beam materials.

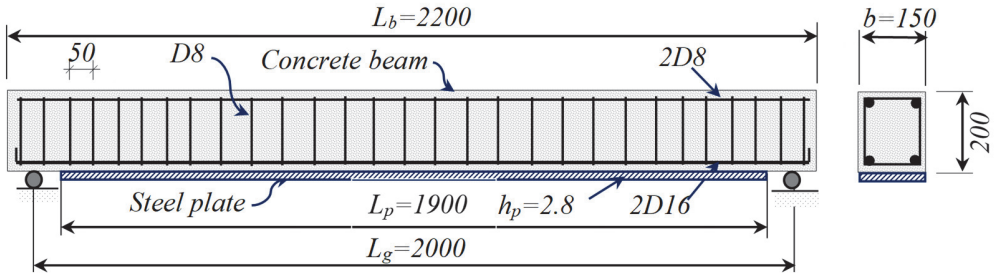

Figure 3: Details of testing RC beams (Dimensions are in mm)

Test Setup and Instrumentation

The four-point bending tests are conducted at the laboratory of the University of Transport and Communications. The tested beam details are presented in Fig. 4. The beam is loaded using a force generator with a loading rate of 0.5 kN/s controlled by a load cell. This load rate is low enough to ensure static loading conditions and negligible dynamic effect. In laboratory conditions, the bearing condition is rigid and assumed to be no displacement, thus one displacement transducer is mounted in the middle of the beam to measure mid-span deflection. The load cell is LRCN 730 1000 from Cooper Instrument & System (US) whose sampling frequency is 30 Hz. As the slip in concrete is the main reason for rupture, however, measuring these stresses in this zone are difficult and may be affected by cracks during bending. Thus, the stresses in steel plates are measured. To determine the stress in the steel plate, three strain gauges are attached to the steel plates. The strain gauge type is KC-60-120-A1-11 provided by Kyowa Strain Gages (Japan). The mounting positions of the strain gauges are at the middle of the span and at 250mm from the ends of the steel plates (Fig. 4). The loading force, beam displacement, and strain are recorded simultaneously based on a control software. This software integrated with sensors is a data logger named SDA 830C of Tokyo Sokki Kenkyujio Co. Ltd (Japan).

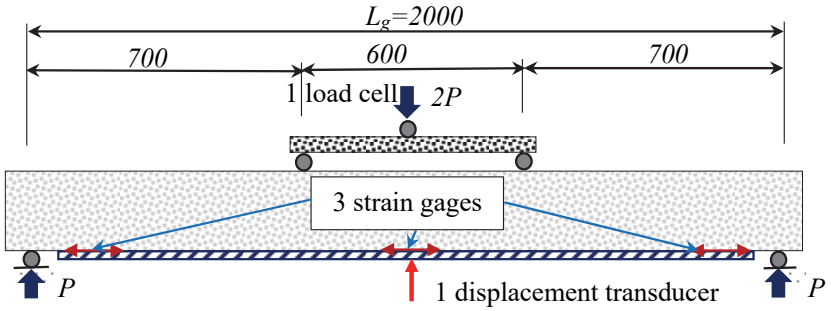

Figure 4: Configuration of the four-point bending test

TEST RESULTS AND DISCUSSIONS

The flexural resistance of the RC beams may be theoretically evaluated as assistant solutions to basically check the test results. Those may be determined based on AASHTO LRFD 2007 [15] for a rectangular section as Eqn. 1.

$$M_n = A_p f_p \left(d_p - \frac{a}{2} \right) + A_s f_y \left(d_p - \frac{a}{2} \right) - A_s' f_y' \left(d_s' - \frac{a}{2} \right) \quad (1)$$

in which, symbols a, d_p, d_s', A_s, A_s' are dimensions and areas are they are defined in Fig. 5, f_p is the stresses in the outer fiber of the steel plate and it is determined by assuming a yield strength of the steel as prescribed by the AASHTO LRFD standards [26] and using the dimension parameters and material properties as given in Fig. 3 and Tab. 1. Based on the flexural moment (in kN.m) in Eq. (1) and the beam configuration as presented in Fig. 4, the corresponding failure force P_f (in kN) can be evaluated accordingly.

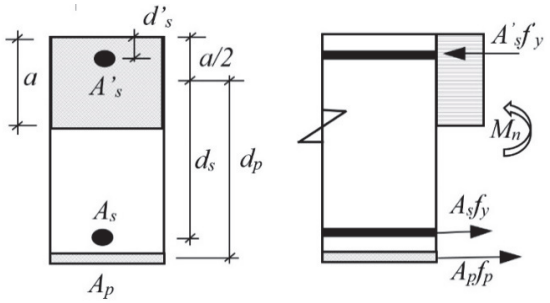

Figure 5: Theoretical bending capacity of the concrete beam section with external steel plate.

The experimental results on the relationship between the measured forces and midspan deflections are presented in Fig. 6. As observed, the beams are subjected to a ductile failure mode and their peak force values are summarized in Tab. 2. Of which, the beams with an external steel plate effectively enhance the flexural strength with an average increase of flexural strength of 85% (Fig. 6 and Tab. 2). For more general failure scenarios, the failure mode and the peak force values based on relatively similar tests by Aykac et al. [3] are also provided in Tab. 2. It is noticed that both brittle and ductile failure modes were observed in [3]. In Fig. 6, the tilt angle of strengthened beams is also larger than that of the referenced beam. This means that the strengthened beam stiffness has been significantly enhanced. Crack distances were measured using a vertical line drawn on the surface of the tested beams. Each vertical lines have a distance of 50mm to determine actual crack distances as shown in Fig. 10. The actual crack distances vary from 48 mm to 212 mm and calculated crack distances are 88 mm and 176 mm. The experimental results of beam deflection in Fig. 6 indicate that the strengthened beams generally have lower ductility than the reference beam. The displacement of the strengthened beam is less than in the reference beam. The experimental results of Aykac and colleagues [3] are even more noticeable. The brittle failure even abrupts in strengthened beams with large thickness plates without special anchorage measures [3]. A simple theoretical model will be proposed in the next section of the present study to consistently predict the brittle or ductile failure modes of the strengthened systems in the present study and those in the study [3].

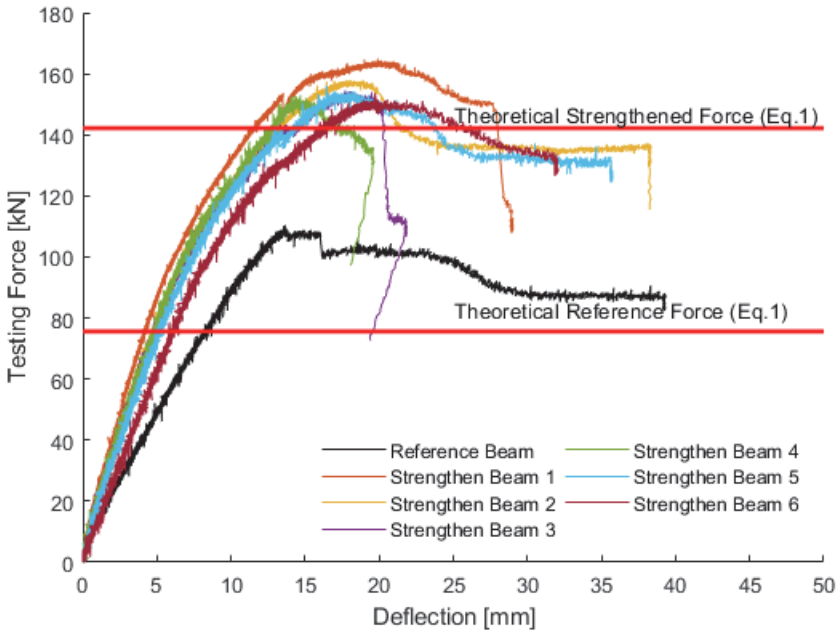

Figure 6: Results of testing forces and deflections.

The measured strains of the external steel plates are presented in Fig. 7 to Fig. 9, corresponding to the left plate end, middle, and right plate end of Beams D1, D2, and D3, respectively. Also, overlaid on the figures are the strains (shown as horizontal lines) based on theoretical models of Raoof's theory [20], an experimental yield strength value, and a proposed value of the present study that will be discussed in the next part of the present study. Generally, it is observed that the beams

are observed to fail in the form of ultimate flexural strength, not be failed by shear failure modes. Also, the stress of the external plate based on Raoof et al. [20] includes the upper and lower threshold stresses. As observed, the range of stress change is smaller than the experimental value. It can be inferred that brittle rupture may be the reason that the stresses in the steel do not reach the yield strength. In the present experimental beams, the beams have been designed, so that brittle failure does not occur but is ductile. Thus, the measured stresses are higher than those predicted by Raoof et al [20].

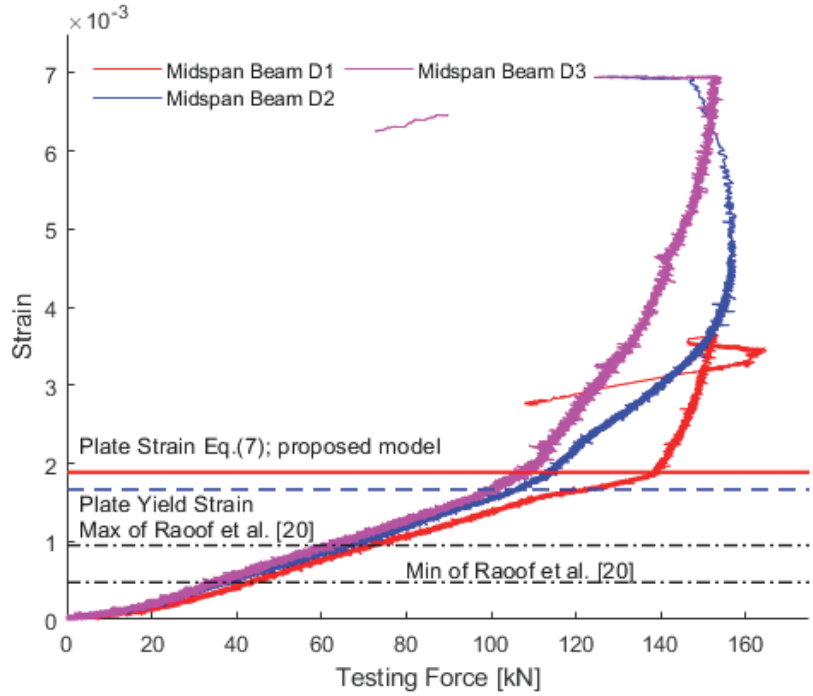

Figure 7: Results of steel plate strain versus testing force at mid span.

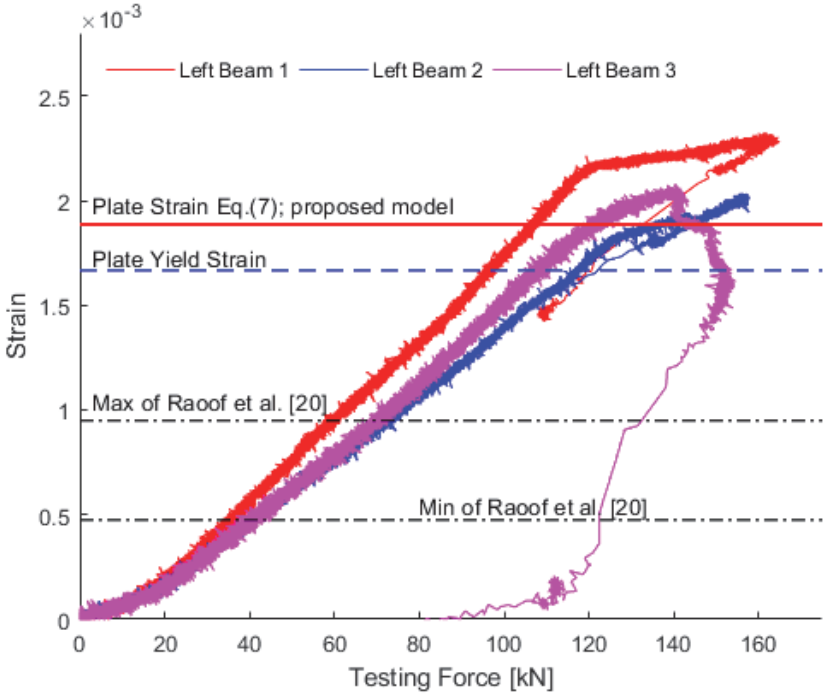

Figure 8: Results of steel plate strain versus testing force at left ends.

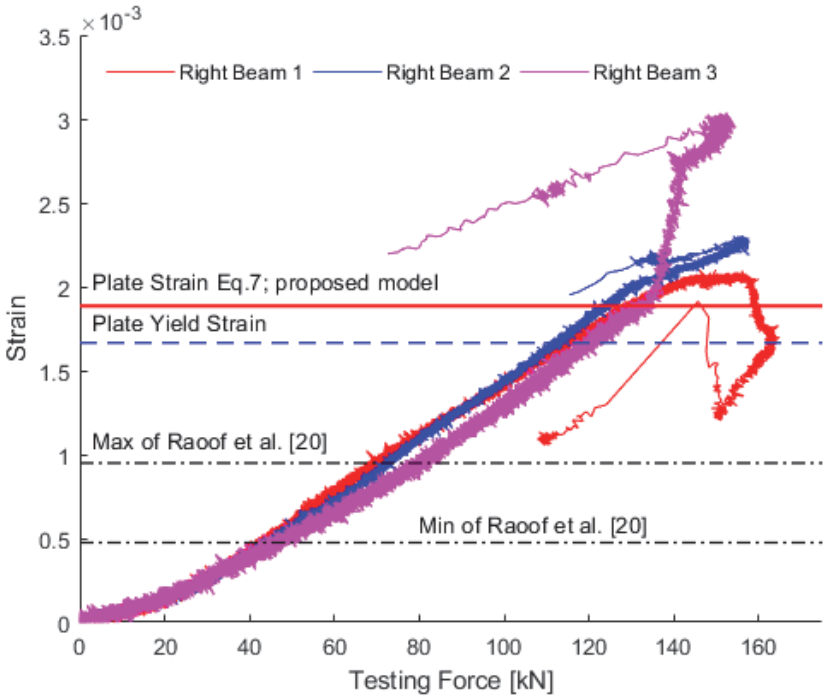

Figure 9: Results of steel plate strain versus testing force at right ends.

The present experimental observations on the beam failure modes show that when a slip crack emerges, the beam immediately fails. The longitudinal sliding position of the external steel also does not automatically appear at the beam end position but it may happen in the middle of the beam, as the sliding of the concrete in the range between successive cracks may happen randomly (Fig. 10). At the large moment location, the distance between the cracks may reach a minimum value, and the slip stresses thus reach a maximum value, conversely, when the cracks may reach a maximum value, and the slip stresses reach a minimum value [3, 20]. As a result, the possibility of sliding along the bending beam is equal. Although the beam configurations were identically made, the beams D1, D3, D5, and D6 have slipped parts at the end of the plates, while beams D2 and D4 have slipped parts in the middle of the plates (Fig. 10). When initial failures occur at one location, they will not happen at other places because the testing force has already begun to decrease.

(a) Failure mode of beam D0: Ductile failure at midspan.

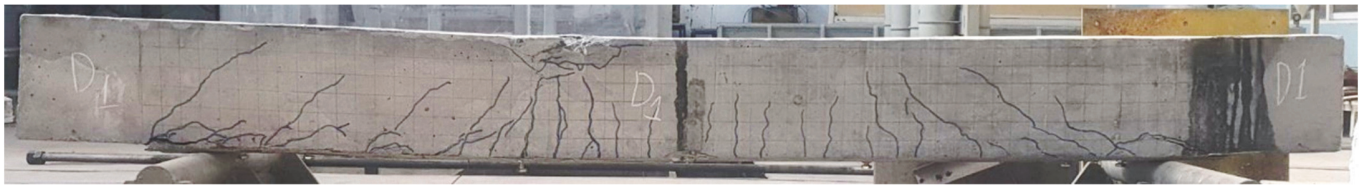

(b) Rupture type of D1: Slip failure at the left end.

(c) Rupture type of D2: Slip failure at middle.

(d) Rupture type of D3: Slip failure at the left end.

€ Rupture type of D4: Slip failure at middle.

(f) Rupture type of D5: Slip failure at the left end.

(g) Rupture type of D6: Slip failure at the left end.

Figure 10: Rupture types of the test beams.

A PROPOSED THEORETICAL SOLUTION FOR THE PREDICTION OF THE BRITTLE/ DUCTILE FAILURE MODES

Stress limit of external steel plate at rupture

In a reinforced concrete beam strengthened with an external steel plate, it is found that the steel plate is usually separated from the beam at a ruptured state in the four-point bending test. This phenomenon frequently occurs as in Fig. 11. Initially, cracks in the concrete beam appear perpendicular to the beam axis, then concrete cracks appear along the beam and happen in the zone between the external steel plate and inner steel bars of the basic beam. This longitudinal crack may appear at the end of the beam or the midspan of the beam. Meanwhile, the outer steel plate does not break. This fracture usually occurs rather suddenly and it is called as a brittle rupture.

No.	Test	Maximum testing force (kN)	Failure mode
1	Beam D0	110.26	Ductile
2	Beam D1	164.95	Ductile
3	Beam D2	157.71	Ductile
4	Beam D3	154.55	Ductile
5	Beam D4	152.74	Ductile
6	Beam D5	155.89	Ductile
7	Beam D6	153.37	Ductile
8	Beam Sbb1.5 [3]	170.00	Ductile
9	Beam Sbb 3 [3]	225.00	Ductile
10	Beam Sb 6 [3]	225.00	Brittle
11	Beam Sb 4.5 [3]	245.00	Brittle
12	Beam Prb6 [3]	229.00	Brittle

Table 2: Maximum testing forces (kN) and failure modes of the present beams and the beams of study [3].

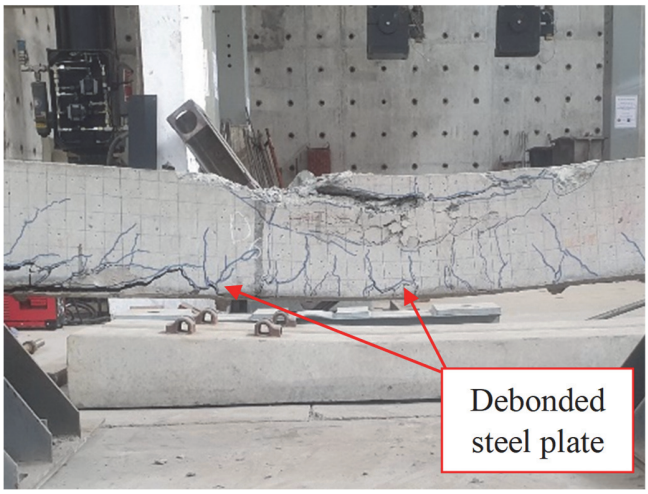

Figure 11: Peeling rupture of steel plate due to concrete sliding.

From the failure mentioned above mode, it is assumed that the shear stress (τ_b) of concrete in the zone between the external steel plate and inner steel bars exceeds the allowable sliding limit (τ_u), and leads to a beam failure. The loss of adhesion between the outer steel and the beam does not occur in the epoxy adhesive because the shear limit in concrete is usually smaller than the shear limit of the epoxy and the shear limit of adhesion between the epoxy layer and steel plate. In the early stages, vertical flexural cracks reduce the shear area of the concrete in the slip direction and thus lead to the slip concentration. When slip occurs, the adhesion between the external plate and the beam is lost. As a result, the external steel plate does not contribute to beam flexural resistance and thus the bending beam immediately reaches its rupture point. This assumption is illustrated in Fig. 12.

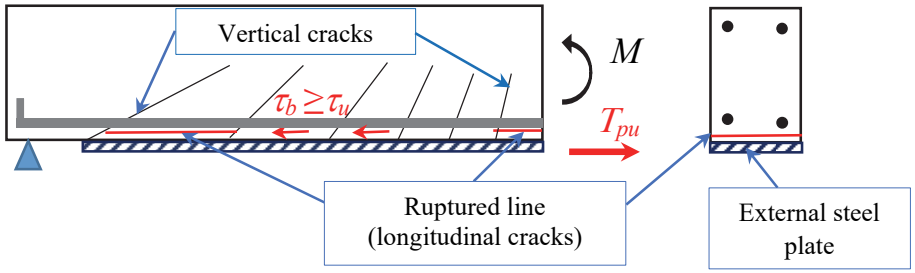

Figure 12: Rupture model in concrete beam with external steel plate.

It is possible to determine the distance between cracks in strengthened concrete beams with external steel plates under flexure by using a "tension chord" theory as introduced by studies [21] [23]. The basic principle is that the total forces exerted by the tensile concrete and steel bars are equal to the sum of the shear slip between the steel and the concrete in the tension zone. Since the outer steel is connected to the beam mainly through adhesion to the concrete at the bottom of the beam, the total tensile force in the tensile part of the beam ($T_c+T_s=A_{ct}f_{ct}+A_sf_y$) shall balance with the total shear force between the concrete, the tensile steel bar, and the external steel plate within the crack range (S). This shear slip (T_p) is the product of the average shear stress between the steel and the concrete (τ_b) with the contact area of concrete and tensile steel (external and internal). This mechanism is illustrated in Fig. 13(a)(c) and Eqn. (2).

$$T_p = \tau_b S \sum U = T_c + T_s \tag{2}$$

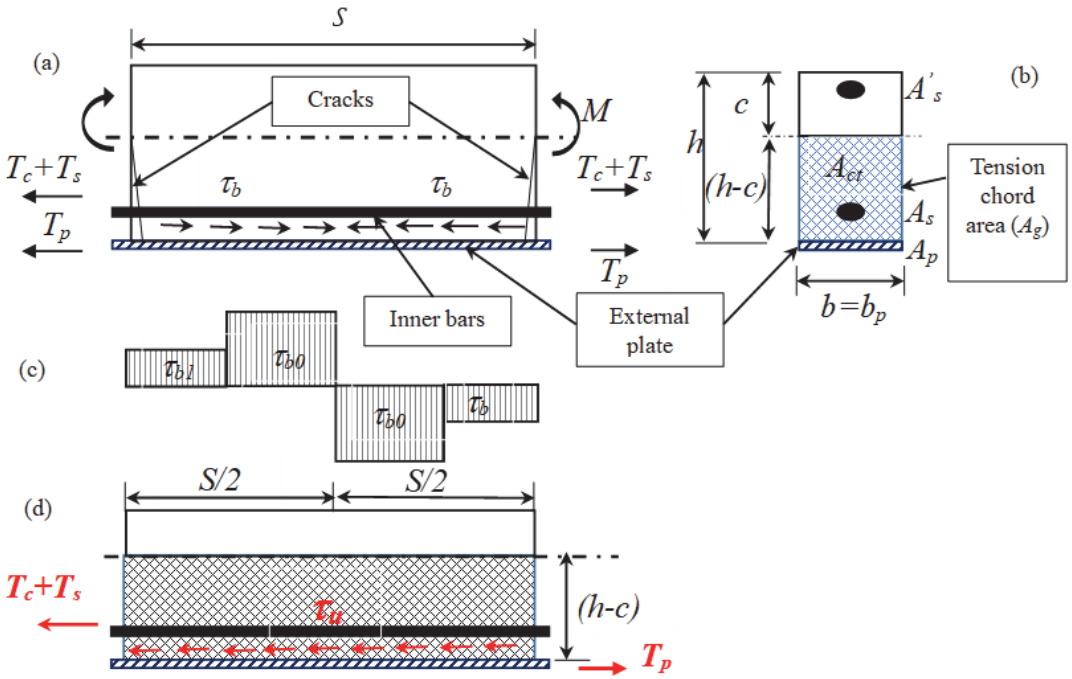

Figure 13: Tension chord model for reinforced beam with external steel plate.

In flexural concrete beams, when a crack appears, the stress state within the concrete where vertical cracks appear will redistribute according to the "tension chord" model. From that point of view, the proposed total area of this "tension chord" for strengthened concrete beams with external steel plates is shown in Fig. 13b. Where c is the height of the concrete compression zone determined as in Eqn. (3).

$$a = \beta_1 c = \frac{A_p f_{py} + A_s f_y - A_s' f_y'}{0.85 f_c' b} \tag{3}$$

where β_1 $\left(\beta_1 = 0.85 - 0.05\left(f_c' - 28\right)/7 \geq 0.65\right)$ is the conversion coefficient corresponding to the height of the compressive concrete area (e.g. AASHTO LRFD [26]). The slip stress distribution (τ_b) before slip failure occurs is assumed as presented in Fig. 13c (in a similar way as proposed by study [21]). The slip strength of concrete maybe τ_u ($\tau_u=\tau_{b0}=2f_{ct}$), in which f_{ct} $\left(f_{ct} = 0.3\sqrt[3]{\left(f_c'\right)^2}\right)$ is the slip resistance of concrete [21] [23]. Insert the tensile steel area ($A_s = \rho_s A_g = n_s \pi d_b^2 / 4$); the tensile concrete area ($A_{ct} = A_g - A_s = \left(1-\rho_s\right) A_g$); the external steel plate area ($A_p = \rho_p A_g = h_p b_p$) into the Eqn. (2), the crack distance (S) can be determined as in Eqn. (4).

$$S = \frac{\left(1-\rho_s\right) f_{ct} + \rho_s f_y}{\tau_b \left(\frac{4\rho_s}{d_b} + \frac{\rho_p}{h_p} \right)} \tag{4}$$

where: the total slipping area between steel and concrete is the product of total contacting circumference ($\sum U$) and crack distance (S). The total contacting circumference $\left(\sum U = n_s \pi d_b + b_p\right)$ is determined by an assumption that inner bars have one nominal diameter.

The maximum distance between cracks (S_{max}) is determined when the slip stress reaches the minimum limit as assumed in Fig. 13c ($\tau_b = \tau_{b1} = f_{ct}$). Insert the slip stress value (τ_b) into Eqn. (4), the maximum crack distance (S_{max}) is in Eqn. (5).

$$S_{\max} = \frac{\left(1-\rho_s\right) + \rho_s \frac{f_y}{f_{ct}}}{\left(\frac{4\rho_s}{d_b} + \frac{\rho_p}{h_p} \right)} \tag{5}$$

The distance between cracks is smallest when the slip stress value reaches to $2f_{ct}$ ($\tau_b = \tau_{b0} = 2f_{ct}$) [21,23]. This distance occurs in areas of the extreme moment when the beam is about to fail. At this stage, the minimum crack distance is assumed as.

$$S_{\min} = S_{\max} / 2 \tag{6}$$

When the beam is in the bending failure stage, the slipping stress between the external steel plate and the base beam (T_p) reaches the maximum value. Due to vertical cracks, the sliding range is limited to the area of two consecutive cracks. Thus, the longitudinal force in the external steel plate can be determined as the total longitudinal shear resistance of the concrete within this crack range $\left(T_p = \tau_b S b_p\right)$. An illustration of this assumption is shown in Fig. 13d. The maximum stresses in the external steel plate can be obtained as

$$f_p = \frac{T_p}{A_p} = \frac{\tau_b S b_p}{A_p} \tag{7}$$

It should be noted that the shear stresses (τ_b) has an equivalent conversion from the diagram in Fig. 13a-d. In the "tension chord" model without external steel, the direction of the slipping stress is derived from the two cracks to the mid-interval. As the external steel plate always tends to slide toward the middle of the beam, the value of τ_b will re-balance with the slipping stress and satisfy Eqn. (2). Thus, a transition to the shear stresses moves in one direction until the failure limit (τ_u) is reached. However, when slip resistance reaches the limit, the slip strength of concrete will fully mobilize. In addition, the values (τ_b) and (S) in Eqn. (7) can be determined in both cases: (1) when $\tau_b = \tau_{b1} = f_{ct}$, then $S = S_{max}$, and (2) when $\tau_b = \tau_{b0} = 2f_{ct}$ then $S = S_{min}$. In both these cases (as well as other intermediate values of τ_b and S) the resulting stresses in the external steel plate are constant. Therefore, longitudinal slip failure can occur randomly at any position in the beam, as illustrated in Fig. 3. Eqn. (7) is the proposed formula to determine the maximum stresses that the steel plate can achieve at the onset of the system failure.

Ductile and brittle rupture conditions

A steel plate-strengthened RC beam is considered to have a ductile failure when the concrete part in compression and tensile steel (including external and internal steel) reaches the yield strength. Due to the aforementioned longitudinal sliding phenomenon, the external steel plate may not reach the yield strength while concrete part and internal steel are already broken. This possibility exposes the beam to brittle failure. When the stress in the external steel plate (in Eqn. (7)) exceeds the yield strength of the steel, the beam is considered as ductile failure. To achieve the ductile requirement, the slip resistance

in the concrete between the two cracks must be sufficiently larger than slip resistance of concrete between two consecutive cracks. Otherwise, the failure mode will be the slip failure of the concrete despite the low external steel stress. In that case, brittle failure will happen. Therefore, ductile failure is only achieved when the external steel stresses is interpreted through Eqn. (7).

$$f_p \geq f_{yp} \tag{8}$$

Insert ($S=S_{max}$) from formula (4) and (f_p) from Eqns. (7), (6) into Eqn. (8) and set the coefficient α_r, the condition for ductile failure in Eqn. (8) is interpreted as in Eqn. (9).

$$\alpha_r = \frac{\left(1-\rho_s\right) f_{ct} + \rho_s f_y}{\left(4\rho_s \dfrac{h_p}{d_b} + \rho_p\right) f_{py}} \geq 1.00 \tag{9}$$

The selection of the external steel plate shall meet Eqn. (9) in order for a strengthened beam not to be subjected to brittle failure. This formula depends not only on the design of the existing beam but also on the mechanical and geometrical properties of the external steel plate to ensure the coefficient of $\alpha_r \geq 1.00$.

VALIDATION OF THE DEVELOPED THEORETICAL MODEL AGAINST EXPERIMENTAL RESULTS

Comparison of stresses at the bottom fiber of the steel plate at the middle span

Fig. 7 has presented the experimentally measured strains at the bottom fiber of the steel plate at the middle span. The experimental results can be divided into two segments, an elastic segment when strains are less than 1.9×10^{-3} and a plastic-elastic segment when strains are greater than that value. Also, overlaid on the figure is the strains of the proposed theoretical solution, as calculated from Eq. (8). It can be observed from the figure that the theoretical strain can approximate the experimental segment-division point (i.e., $\approx 1.9\times10^{-3}$). Similar observations can be obtained from the comparisons of the measured strains and the predicted stresses based on Eq. (6) for the strains at the bottom fiber of the steel plate at the left span (Fig. 8) and those at the right span (Fig. 9). This indicates that the theoretically calculated strains in Eqn. (8) can excellently capture the experimentally measured segment-division points in the steel plate.

Comparison of crack distances

Tab. 3 presents the comparison of the predicted minimum/maximum crack distances and the failure mode between the present theoretical solutions and the expertimental results of the present study. For the theoretical solution, the minimum to maximum crack distances can be evaluated based on Eqs. (6) and (7). For beams D1-D6, the crack distances are evaluated as 88 mm and 176 mm, respectively. Meanwhile, the actual crack distantces of the present experimental studies are ranged from 48 mm to 212 mm (as observed in Fig. 10**)**. It is noted that in each test girder, grid line were marked to measure crack spacing. It was shown that the mechanism illustrated in Eqn. (3) can excellently predict the crack distances of RC concrete beams with external steel plates.

Location of the steel plate delamination

As shown in Fig.10, there are two plate-strengthened RC beams those are delaminated at the beam midspan (i.e., speciments D2 and D4). On the other hand, four other plate-strengthened RC beams are delaminated at the ends of the steel plate. This phenomenon agrees with theoretical analysis results as discussed above (i.e.,Eq. (7)). The evaluation of steel plate stresses is independent on either crack spacing or position of crack and delamination. Based on the present proposed theoretical model, maximum and minimum crack distances can be evaluated as indicated in Eqs. (5),(6) and from that, the prediction of the stresses of the steel plate can be determined (i.e., Eq. (7)). As a result, the randomness of crack position, crack distance, and position of delamination can be handled.

Comparison of the system failure modes

As the displacement of the strengthened beam (i.e., D1-D6) is less than in the reference beam (i.e., D0). The experimental results of beam deflection in Fig. 6 indicate that the strengthened beams generally have lower ductility than the reference

beam. The experimental results of Aykac et al. [3] in Fig. 1 are even more noticeable. The brittle failure even abrupts in strengthened beams with large thickness plates without special anchorage measures. For the theoretical solutions, the ductile or brittle failure modes can be predicted by using Eq. (10). Tab. 3 presents the ductile/brittle failure modes as observed from the present experimental beams (D1-D6) and the experimental studies of Aykac et al. [3]. It can be observed from the table that the theoretical predictions excellently capture the experiment failure modes. It is here noted that the failure type of the beam is observed to depend on both the reference beam details and external steel plate parameters. These parameters include the dimensions and material properties. Generally, the addition of external steel tends to increase the brittleness of the structure and reduce the total deflection of strenthenned beam. Therefore, the theoretical prediction using Eq. (10) is proposed to select the appropriate external steel ratio for the existing beam to ensure ductility. Although the present theoretical results are well validated against the present experimental results as well as the experiment results by Aykac et al. [3], it is also recommended that further investigations against other beam configurations should be required to achieve better validations.

		Theoretical predictions				Experiment results	
No.	Test	Predicted minimum/maximum crack distance (mm)	Predicted stress in steel plate at rupture (Eq. (8))	Coefficient α_r (Eq. (10))	Theoritical results of rupture type	Actual minimum/maximum crack distance (mm)	Experiment results of rupture type
1	Present beam D1	88/176	389.8	1.03 > 1	Ductile	45/150	Ductile
2	Present beam D2	88/176	389.8	1.03 > 1	Ductile	60/280	Ductile
3	Present beam D3	88/176	389.8	1.03 > 1	Ductile	60/210	Ductile
4	Present beam D4	88/176	389.8	1.03 > 1	Ductile	60/200	Ductile
5	Present beam D5	88/176	389.8	1.03 > 1	Ductile	100/200	Ductile
6	Present beam D6	88/176	389.8	1.03 > 1	Ductile	50/180	Ductile
7	Beam Sbb1.5 [3]	124/248	848.95 (ruptured)	3.03 > 1	Ductile	N/A	Ductile
8	Beam Sbb 3 [3]	120/241	412.80 (ruptured)	1.47 > 1	Ductile	N/A	Ductile
9	Beam Sb 6 [3]	114/227	194.71	0.70 < 1	Brittle	N/A	Brittle
10	Beam Sb 4.5 [3]	117/234	267.4	0.96 < 1	Brittle	N/A	Brittle
11	Beam Prb6 [3]	114/227	194.71	0.70 < 1	Brittle	N/A	Brittle

Table 3: Comparison of the failure modes of plate-strengthened RC beams between the proposed theoretical model against experimental results.

CONCLUSION

An experimental study and a proposed theoretical solution were conducted in the present study to investigate the ductile/ brittle failure mode of reinforced concrete beams strengthened with an external steel plate. Six steel plate-strengthened RC beams and one non-strengthened RC beam have been fabricated and tested under 4-point bending loads. The experimental study showed that the failure mode was based on concrete sliding along with the external plate. This slip was limited between two vertical cracks, from which the maximum stress in the external steel was determined. The proposed theoretical model was then developed based on the observed experimental results to analyze the crack formation, to determine the distance between vertical cracks, and to quantitatively predict the ductile/brittle failure mode of plate-

strengthened RC beams. It was observed from the study that the maximum tensile force in the external steel plate was equal to the slip resistance of the concrete within the consecutive vertical cracks from which the maximum stress at failure was determined. If this stress value exceeded the yield limit, the beam was considered as a ductile failure and thus a coefficient of the threshold for ductile failure could be determined.

Most of the beams reinforced with an external steel plate is prone to brittle failure. Therefore, it is necessary to calculate the steel quantity to ensure that this does not occur in the strengthening design. Based on this study, the external plate size can be selected to meet the load upgrade needs without causing brittle failure follows Eqn. (9). In the case of irreparable brittle failure, the stresses in the outer steel will be less than the yield strength. Thus the bending capacity will be reduced and can be evaluated using this study in Eqn. (7). The present study has conducted and discussed excellent validations of these theoretical equations against experimental results.

Through the observed experimental and the analytical results, two important conclusions have been found in the present study. The first conclusion is that the steel plate separation is random, i.e., it can occur at the end or at an intermediate location of the steel plate. Based on the present proposed theoretical model, the minimum and maximum distances between two cracks can be predicted. From that, it is possible to determine the stresses in the external steel plate at the onset of the system failure without taking care to specifying the positions of cracks and delamination. The second conclusion is that the present theoretical model is relatively simple, quick to predict the brittle/ductile failure mechanism of the steel plate-strengthened RC beams and thus it may be convenient to control the ductile behavior at the ultimate bending state of such strengthened systems.

NOTATION

A_c	Tensile area of concrete
A_p	Area of external steel plate
A_s	Area of internal steel bars
$A_g = A_c + A_s$	Gross area of tension chord
A'_s	Area of compressive bars
S	Crack spacing
$S_{\min}$	Minimum crack spacing
$S_{\max}$	Maximum crack spacing
$\sum U$	Total adhesion circumference between steel and concrete
c	Distance from the extreme compression fiber to the neutral axis (mm)
$a = \beta_1 c$	Equivalent distance from the extreme compression fiber to the beam neutral axis (mm)
d_b	Diameter of tensile bars
d_p	Distance from the extreme compression fiber to the neutral axis of steel plate
f_{ct}	Tensile strength limit of concrete
f'_c	Compressive strength of concrete (MPa, specimen type D=150mm, H=300mm)
f_p	Tensile stress in external steel plate
n_s	Number of tensile steel bars
α_r	Coefficient to determine ductility of strengthenned beam
β_1	Ratio of the depth of the equivalent uniformly stressed compression zone assumed in the strength limit state to the depth of the actual compression zone
$\rho_s = A_s / A_g$	Ratio of tensile steel bar area to total tensile area zone
$\rho_p = A_p / A_g$	Ratio of external steel plate area to total tensile area zone
τ_b	slip stress in concrete along tensile steel
RC	Reinfored Concrete

REFERENCE

[1] Zou, X., Lin, H., Feng, P., Bao, Y., and Wang, J. (2021). A review on FRP-concrete hybrid sections for bridge applications. Composite Structures, 262, pp. 113336. DOI: 10.1016/j.compstruct.2020.113336

[2] Rakgate, S. M. and Dundu, M. (2018). Strength and ductility of simple supported R/C beams retrofitted with steel plates of different width-to-thickness ratios. Engineering Structures, 157, pp. 192–202. DOI: 10.1016/j.engstruct.2017.12.012

[3] Aykac, S., Kalkan, I., Aykac, B., Karahan, S., and Kayar, S. (2013). Strengthening and Repair of Reinforced Concrete Beams Using External Steel Plates. Journal of Structural Engineering, 139 (6), pp. 929–939. DOI: 10.1061/(ASCE)ST.1943-541X.0000714

[4] Neto, P., Alfaiate, J., and Vinagre, J. (2014). A three-dimensional analysis of CFRP–concrete bond behaviour. Composites Part B: Engineering, 59, pp. 153–165. DOI: 10.1016/j.compositesb.2013.11.025

[5] Gul, Akhtar; Alam, Bashir; Ahmed, Wisal; Wahab, Nauman; Shahzada, Khan; Irfan Badrashi, Yasir; Wali Khan, Sajjad; Khan, Muhammad Nasir Ayaz (2020). Strengthening and Characterization of Existing Reinforced Concrete Beams for Flexure by Effective Utilization of External Steel Elements. Advances in Structural Engineering, 1-9. DOI: 10.1177/1369433220950614

[6] Mohamed Ali, M. S., Oehlers, D. J. and Bradford, M. A. (2005). Debonding of steel plates adhesively bonded to the compression faces of RC beams. Construction and Building Materials, 19(6), 413–422. DOI: 10.1016/j.conbuildmat.2004.11

[7] Wu, Y.-F. and Lu, J. (2013). Preventing debonding at the steel to concrete interface through strain localization. Composites Part B: Engineering, 45(1), 1061–1070. DOI:10.1016/j.compositesb.2012.08

[8] Sallam, H. E.-D. M., Saba, A.-A. M., Shahin, H. H. and Abdel-Raouf, H. (2004). Prevention of Peeling Failure in Plated Beams. Journal of Advanced Concrete Technology, 2(3), 419–429. DOI:10.3151/jact.2.419

[9] Leung, Christopher K. Y.. (2001). Delamination Failure in Concrete Beams Retrofitted with a Bonded Plate. Journal of Materials in Civil Engineering, 12(2), 106-113. DOI: 10.1061/(ASCE)0899-1561(2001)13:2(106)

[10] Batti, M., Silva, B., Piccinini, Â., Godinho, D. and Antunes, E. (2018). Experimental Analysis of the Strengthening of Reinforced Concrete Beams in Shear Using Steel Plates. Infrastructures, 3(4), 52. DOI: 10.3390/infrastructures3040052.

[11] Napoli, A. and Realfonzo, R. (2015). Reinforced concrete beams strengthened with SRP/SRG systems: Experimental investigation. Construction and Building Materials, 93, 654–677. DOI: 10.1016/j.conbuildmat.2015.06.

[12] Mertoğlu, Ç., Anil, Ö. and Durucan, C. (2016). Bond slip behavior of anchored CFRP strips on concrete surfaces. Construction and Building Materials, 123, 553–564. DOI: 10.1016/j.conbuildmat.2016.07.

[13] Zhang, P., Lei, D., Ren, Q., He, J., Shen, H. and Yang, Z. (2020). Experimental and numerical investigation of debonding process of the FRP plate-concrete interface. Construction and Building Materials, 235, 117457. DOI: 10.1016/j.conbuildmat.2019.11

[14] Liu, Y., Zhang, M., Yin, X., Huang, Z. and Wang, L. (2019). Debonding Detection of Reinforced Concrete (RC) Beam with Near-Surface Mounted (NSM) Pre-stressed Carbon Fiber Reinforced Polymer (CFRP) Plates Using Embedded Piezoceramic Smart Aggregates (SAs). Applied Sciences, 10(1), 50. DOI: 10.3390/app10010050

[15] Wojtczak, E., Rucka, M. and Knak, M. (2020). Detection and Imaging of Debonding in Adhesive Joints of Concrete Beams Strengthened with Steel Plates Using Guided Waves and Weighted Root Mean Square. Materials, 13(9), 2167. DOI: 10.3390/ma13092167

[16] Al-Saadi, N. T. K., Al-Mahaidi, R. and Abdouka, K. (2016). Bond behaviour between NSM CFRP strips and concrete substrate using single-lap shear testing with cement-based adhesives. Australian Journal of Structural Engineering, 17(1), pp. 28–38. DOI: 10.1080/13287982.2015.1116180

[17] Ceroni, F., Pecce, M., Matthys, S., and Taerwe, L., (2201), Debonding strength and anchorage devices for reinforced concrete elements strengthened with FRP sheets. Composites: Part B (39), pp. 429–441. DOI: 10.1016/j.compositesb.2007.05.002

[18] J. Chen, F. and Teng, J. G. (2001). Anchorage Strength Models for FRP and Steel Plates Bonded to Concrete. Journal of Structural Engineering, 127(7), pp. 784–791. DOI: https://doi.org/10.1061/(ASCE)0733-9445(2001)127:7(784)

[19] ACI Committee 440.2R-17. (2017). Guide for the Design and Construction of Externally Bonded FRP Systems for Strengthening Concrete Structures. https://www.concrete.org/store/productdetail.aspx?ItemID=440217&Language=English&Units=US_AND_METRIC

[20] Raoof, M., El-Rimawi, J. A. and Hassanen, M. A. H. (2000). Theoretical and experimental study on externally plated R.C. beams. Engineering Structures, 22(1), pp. 85–101. DOI: 10.1016/S0141-0296(98)00056-X

[21] Marti, P., Alvarez, M., Kaufmann, W. and Sigrist, V. (1998). Tension Chord Model for Structural Concrete. Structural Engineering International, 8(4), pp. 287–298. DOI: 10.2749/101686698780488875
[22] Kaklauskas, Ramanauskas, G., R. and Ng, P.L. (2019). Predicting Crack Spacing of Reinforced Concrete Tension Members Using Strain Compliance Approach with Debonding. Journal of Civil Engineering and Management, 25(5), pp. 422–430. DOI: 10.3846/jcem.2019.9871
[23] Gilbert, R. I., (2008). Control of Flexural Cracking in Reinforced Concrete. ACI Structural Journal, 105-S29, pp. 301-307. https://www.concrete.org/publications/internationalconcreteabstractsportal/m/details/id/19789
[24] Nguyen, V.H., (2020). Study of Rupture Mechanism in Concrete Girder Strengthened by External Fiber Reinforced Polymer Using Crack Analysis. IOP Conference Series: Materials Science and Engineering: Materials Science and Engineering, 869, pp. 072069. https://iopscience.iop.org/article/10.1088/1757-899X/869/7/072049
[25] American Assossiation of State Highway and Transportation Officials. (2017). AASHTO LRFD Bridge Design Specifications. SI Units, 8th Edition. https://trid.trb.org/view/1488438
[26] ASTM A370-15 (2016). Standard Test Methods and Definitions for Mechanical Testing of Steel Products. DOI: 10.1520/A0370-16
[27] ASTM C39 (2021). Standard Test Method for Compressive Strength of Cylindrical Concrete Specimens. DOI: https://www.astm.org/c0039_c0039m-21.html
[28] Bafekrpour, Ehsan. Advanced Composite Materials: Properties and Applications, Warsaw, Poland: De Gruyter Open Poland, 2017. DOI: 10.1515/9783110574432
[29] Patcharaphun, S., (2006), Characterization and Simulation of Material Distribution and Fiber Orientation in Sandwich Injection Molded Parts, Ph.D. thesis, Institute of Mechanical and Plastics Engineering, Chemnitz University of Technology.